RSC Advances

PAPER

View Article Online
View Journal | View Issue

Cite this: *RSC Adv.*, 2023, **13**, 15121

BODIPY-based near-infrared semiconducting polymer dot for selective yellow laser-excited cell imaging†

Lei Chen, [ab] Yifei Jiang, [b] Shihan Xu,[b] Jicheng Zhang,[b] Seung-Ryoung Jung,[b] Jiangbo Yu, [b] Xuanjun Zhang [c] and Daniel T. Chiu*[b]

Semiconducting polymer dots (Pdots) with both narrow-band absorption and emission are desirable for multiplexed bioassay applications, but such Pdots with absorption peaks beyond 400 nm are difficult to achieve. Here we describe a donor–energy transfer unit–acceptor (D–ETU–A) design strategy to produce a BODIPY-based Pdot that exhibits simultaneously narrow absorption and emission bands. A green BODIPY (GBDP) unit was employed as the main building block of the polymer backbone, conferring a strong, narrow-band absorption around 551 nm. An NIR720 acceptor provides narrow-band NIR emission. The small Stokes shift of the GBDP donor allows introduction of a benzofurazan-based ETU, resulting in a ternary Pdot with a fluorescence quantum yield of 23.2%, the most efficient yellow-laser excitable Pdot. Due to the strong absorbance band centered at 551 nm and weak absorbance at 405 nm and 488 nm, the Pdot showed high single-particle brightness when excited by a 561 nm (yellow) laser, and selective yellow laser excitation when used to label MCF cells, with much greater brightness when excited at 561 nm than at 405 nm or 488 nm.

Received 17th February 2023
Accepted 25th April 2023

DOI: 10.1039/d3ra01083j

rsc.li/rsc-advances

1. Introduction

Semiconducting polymer dots (Pdots) are a class of small (usually < ~30 nm) fluorescent probes for *in vitro* and *in vivo* imaging, biosensors, optical theranostics, and other biomedical applications.[1–17] Pdots provide ultrahigh brightness,[18,19] excellent photostability,[20,21] low cellular toxicity,[22] good water dispersibility, tunable photophysical properties, and easy bioconjugation.[23] Pdots are also capable of multi-color emission at the single-particle level, with tunable relative fluorescence intensities,[24] a capability that is useful for developing spectrally-barcoded probes for multiplexed assays. However, the design of such probes is limited by the availability of fluorophores with distinct excitation and emission. We previously developed a series of Pdots with narrow-band emission by incorporating green and red BODIPY dyes into a blue-emitting polyfluorene (PF) backbone.[25] By adjusting the relative content of the narrow-emission BODIPY dyes in the backbone, a set of 20 spectral-intensity-encoded Pdots with 405 nm laser excitation were obtained for cell barcoding and tracking.[26] However, it is difficult to obtain many more Pdot barcodes by simply increasing the fluorescent components due to the emissive spectra overlap problem.

The number of Pdot barcodes available for multiplex assays could be further increased by integrating additional Pdots with narrow absorption near other commonly used laser sources (488, 561, and 633 nm). For example, by designing another set of 20 Pdot barcodes which can be excited by a 561 nm laser while exhibiting weak fluorescence when excited by a 405 nm laser, the number of fluorescence-encoded cells in a single detection could be doubled. One limitation of existing Pdots is their broad absorption bands,[27,28] which result in comparable emission intensities when excited by different light sources. Another limitation is the lack of bright, long-wavelength excitable (LWE) Pdots (λ_{abs} > 520 nm). Blue laser (405 or 488 nm)-excitable PF- or PFBT-based Pdots with high fluorescence quantum yield (Φ_f > 30%) have been achieved,[29–31] but most LWE Pdots have shown low Φ_f (<10%),[28,32–36] mainly due to aggregation-induced self-quenching in the solid-like Pdot state. A few LWE conjugated polymer nanoparticles with higher Φ_f have been reported,[37,38] but these approaches have often involved dilution of the conjugated polymer content in the nanoparticles.

Therefore, there remains a need for bright LWE Pdots with narrow-band absorption and emission, with λ_{abs} near the commonly-used laser excitation wavelengths of 561 nm or 633 nm. Here we employ a donor–energy transfer unit–acceptor

[a]*Department of Biomedical Engineering, Sun Yat-Sen University, Shenzhen, 518107, China*

[b]*Department of Chemistry and Bioengineering, University of Washington, Seattle, Washington, 98195, USA. E-mail: chiu@uw.edu*

[c]*Department of Health Sciences, University of Macau, Taipa, Macau SAR, 999078, China*

† Electronic supplementary information (ESI) available. See DOI: https://doi.org/10.1039/d3ra01083j

(D–ETU–A) design strategy with the novel use of a BODIPY unit as the predominant building block of a Pdot polymer backbone to produce LWE (561 nm) Pdot with simultaneously narrow absorption and emission bands, a large Stokes shift (165 nm), and a high fluorescence quantum yield ($\Phi_f = 23.2\%$).

2. Results and discussion

As shown in Fig. 1, the designed ternary D–ETU–A copolymer, PFBDP-NIR720 (P1), is composed of a green emissive BODIPY (GBDP) unit as predominant light absorber (D), 4,7-bis(4-octyloxy-2-thienyl)-2,1,3-benzooxadiazole (DOTBO) as the ETU, and a previously reported NIR720 emitter[18] as the acceptor (A).

The corresponding P1 Pdots were obtained by using a nano-precipitation method developed previously in our lab.[31] Briefly, as shown in Fig. 1, conjugated polymer was co-dissolved with an optimized amount (20 wt%) of the amphiphilic polymer carboxyl-functionalized polystyrene-*g*-poly(ethylene oxide) (PS-PEG-COOH) in tetrahydrofuran (THF), and the mixture was quickly injected into Di-water under sonication. Organic THF solvent was then removed by blowing nitrogen gas into the mixture at ~70 °C. The resulting solution was filtered with a 0.22 μm cellulose membrane filter to remove aggregates to obtain a Pdot solution at 0.01 mg mL^{-1}.

The GBDP unit was chosen as the main building block because in its core structure, the coordination of the boron atom holds the dipyrromethene ligand in a highly rigid and planar conformation, giving GBDP a sharp and intense absorption band with a peak at around 500 nm, which is

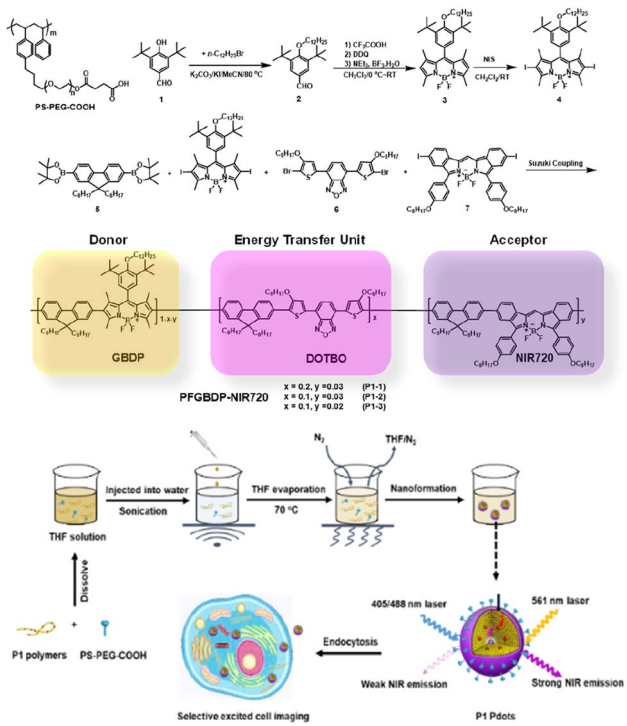

Fig. 1 The chemical structure of PS-PEG-COOH and synthesis routes of P1 polymers. And the schematic illustration of P1 Pdot formation and its application for selective excited cell imaging.

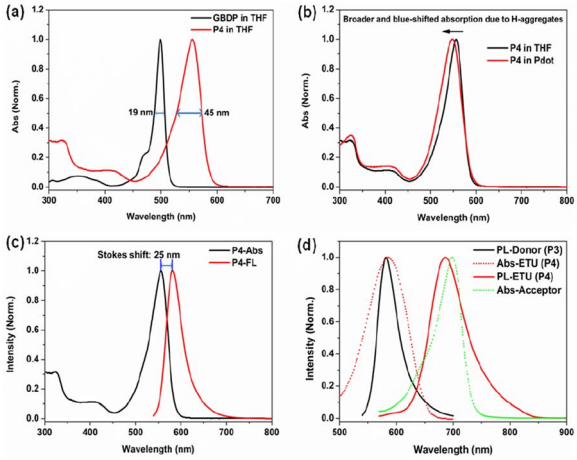

Fig. 2 (a) Absorption spectra of GBDP dye and PFBDP polymer (P4) in diluted THF solution; (b) absorption spectra of P4 in THF and in the Pdot state; (c) Stokes shift of P4 in THF solution; (d) spectral overlap of donor emission and ETU absorption, and of ETU emission and acceptor absorption.

attributed to the S_0–S_1 (π–π^*) transition. The full width at half maximum of this main absorption band ($FWHM_{abs}$) is as small as 19 nm (Fig. 2a). Relatively weaker broad absorption bands in the shorter wavelength region can be assigned to the S_0–S_n ($n \geq 2$) (π–π^*) transition.[39] Due to the strong and narrow absorption of the BODIPY core, its alternative copolymer derivatives usually exhibit a narrow and S_0–S_1 transition-dominated absorption band as well.[40–43]

The GBDP segment was alternatively copolymerized with 9,9-dioxylfluorene to form PFBDP (P4, Scheme S1†), acting as the predominant absorber in the P1 Pdot. Pure P4 polymer in diluted THF solution exhibits a pronounced bathochromic shift of the absorption maximum (57 nm) relative to the initial GBDP dye because of its significant extension of π-conjugation (Fig. 2a). In addition, the main absorption band of the P4 polymer becomes broader than that of GBDP dye (45 nm *vs.* 19 nm) as a result of the extended π-conjugation and reduced molecular rigidity.[43] Compared to P4 polymer in THF, P4 Pdot in aqueous solution shows a broader S_0–S_1 absorption band ($FWHM_{abs}$: 57 nm *vs.* 45 nm) and a much lower Φ_f (1.2% *vs.* 65.6%) due to formation of non-emissive H-aggregates (Fig. 2b).

To obtain an efficient PFBDP-based Pdot, it was necessary to introduce an energy-transfer unit to compete with H-aggregates and to maximally capture the excitation energy of PFBDP. The small Stokes shift of P4 (25 nm, in THF solution) (Fig. 2c) provided sufficient spectral width to add the DOTBO ETU, which was selected due to its ideal spectral overlap with the PFBDP energy donor and NIR720 acceptor (Fig. 2d). A small amount of NIR720 was incorporated into the polymer backbone, resulting in the ternary D–ETU–A P1 polymer. Three P1 variants with different ETU and NIR720 composition (recording based on the feeding ratios) were characterized: P1-1 (20 mol% ETU, 3 mol% NIR720), P1-2 (10 mol% ETU, 3 mol% NIR720), and P1-3 (10 mol% ETU, 2 mol% NIR720) (Fig. 1).

The properties of the three P1 variant Pdots are listed in Table 1. The three Pdots showed an average diameter of 21–

Table 1 Photophysical properties and diameters by DLS of there P1 Pdots

Pdot	λ_{abs} [nm]	λ_{PL} [nm]	Φ_f [%]	Size [nm]
P1-1	550	715	14.5	22.5
P1-2	551	715	23.2	21.8
P1-3	551	715	19.8	24.6

25 nm based on dynamic light scattering (DLS). Of the three P1 variants, P1-2 exhibited the best performance, with the highest Φ_f (23.2%), lowest relative absorption intensity in the UV/blue region, and most complete energy transfer from the ETU to the NIR720 emitter (Fig. S1†). The Φ_f of P1-x series Pdots is determined by the trade-off between energy transfer efficiency and aggregation-induced fluorescence quenching. The light absorbed by PFGBDP host cannot be fully utilized with low ETU and NIR720 emitter content. On the other hand, high ETU and NIR720 emitter content will lead to aggregation-induced fluorescence quenching. The P1-2 Pdot with a feeding ratio of $x = 0.1$ and $y = 0.03$ optimized this trade-off. Based on these results, P1-2 Pdot was selected for further characterization.

As shown in Fig. 3a, the number-average diameter of hydrated P1-2 Pdot was ~22 nm evaluated by DLS. Fig. 3b shows the profile of dried P1-2 Pdot on cupper mesh substrate by high-resolution transmission electron microscopy. The P1-2 Pdot has a dominant narrow absorption band with λ_{abs} at 551 nm, close to the 561 nm laser source (Fig. 3c). The $FWHM_{abs}$ of P1-2 is only 56 nm, much narrower than that of PFBT-NIR720 (P2, 104 nm) and PFDHTBT-NIR720 (P3, 112 nm), which are commonly used in NIR Pdots (Fig. S2†).[18] Compared to the pure P4 Pdot, the relative absorbance of the P1-2 Pdot in the short wavelength region (300–450 nm) is slightly stronger, mainly because of the introduction of the DOTBO unit, but is still much lower than that of existing non-BODIPY-based Pdots. The building blocks used in previously reported Pots include extended π-conjugated repeated units (such as PPV derivatives), and strong electron donating and electron withdrawing repeated units (such as PFDHTBT). These types of polymers have non-rigid and twisted molecular structures, and usually exhibit a broader and relatively weaker S_0–S_1 (π–π* transition or intramolecular charge transfer) absorption band in the longer wavelength region than our P1 polymers. Because of the excellent spectral overlap of the D/ETU and ETU/A in P1-2, sufficient cascade energy transfer occurred to produce a narrow emission band with a $FWHM_{emi}$ of 46 nm.

The GBDP unit also gives the P1-2 Pdot a larger molar extinction coefficient (ε) than that of existing NIR Pdots. The maximum absorbance (A_{max}) of the P1-2 Pdot at 0.005 mg mL^{-1} is 0.3, ~1.9 times that of the PFBT-based Pdot and 2.7 times that of the PFDHTBT-based Pdot (Table S1†). Because single-particle brightness is proportional to the product of absorption cross-section and Φ_f, higher ε leads to a brighter Pdot. Single-particle fluorescence imaging of P1-2 Pdots was acquired by using a wide-field total internal reflection (TIRF) microscope (Fig. 3d), with a mean-averaged single-particle brightness of 3.0×10^3 photons per frame. The P1-2 Pdot also exhibits a large Stokes shift of 165 nm, a favourable feature for minimizing fluorescence noise from the excitation source.

To further evaluate the brightness of the P1-2 Pdot, we compared it with that of a currently used fluorescence probe

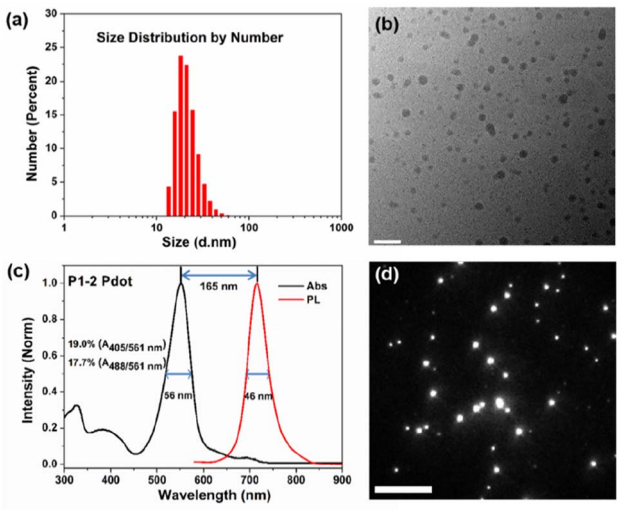

Fig. 3 Characterization of P1-2 Pdot, the best performing of the three P1 Pdot variants. (a) and (b) Size distribution characterized by DLS (a) and TEM (b, scale bar = 100 nm); (c) absorption and emission spectra; (d) single-particle fluorescence imaging using a wide-field total internal reflection fluorescence microscope (scale bar = 100 μm).

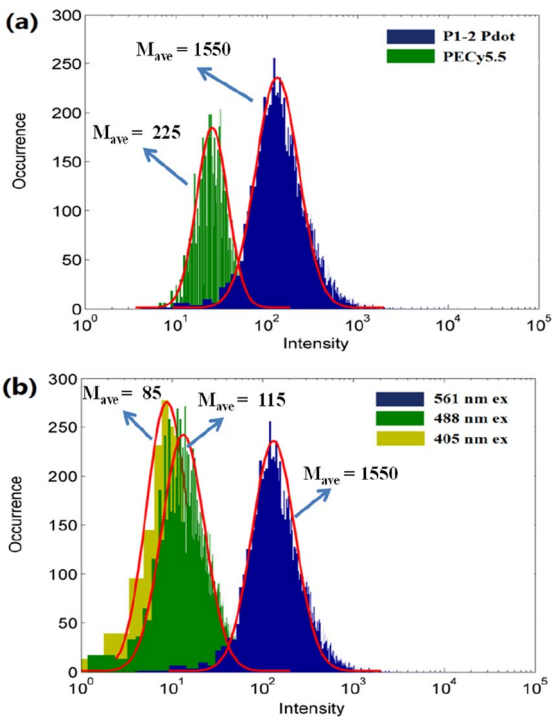

Fig. 4 Single-particle brightness of (a) the P1-2 Pdot and PE-Cy5.5 excited using a 561 nm laser, and (b) the P1-2 Pdot excited using 405, 488, and 561 nm lasers.

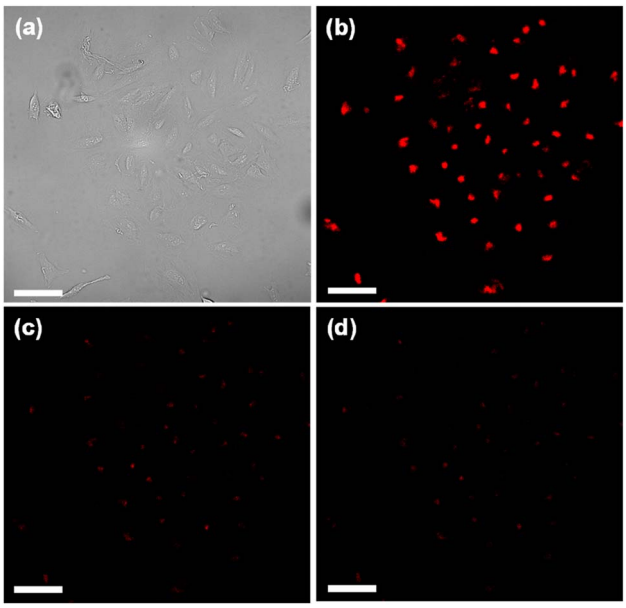

Fig. 5 Confocal fluorescence microscopy images of MCF-7 cells labeled with the P1-2 Pdot (scale bar = 50 μm): (a) bright-field image, and corresponding fluorescence images with laser excitation at (b) 561 nm, (c) 488 nm, and (d) 405 nm, showing selective excitation at 561 nm.

PE-Cy5.5. The absorption and fluorescence spectra of PE-Cy5.5 are shown in Fig. S3.† The single-particle brightness of the P1-2 Pdot and PE-Cy5.5 were assessed by using a custom single-particle flow analyzer.[44] Using this system and 561 nm laser excitation, the mean single-particle brightness of the P1-2 Pdot is ~6.8 times that of the PE-Cy5.5 probe (Fig. 4a). The main purpose in designing the P1-2 polymer was to obtain a bright Pdot which can be selectively excited by a 561 nm laser. Therefore, we also acquired the single-particle brightness of the P1-2 Pdot when excited by 488 nm and 405 nm lasers at the same laser power density. The mean brightness ratios were 13.4 for $I_{561\ nm}/I_{488\ nm}$ and 18.2 for $I_{561\ nm}/I_{405\ nm}$, indicating minimal cross excitation at 405 nm and 488 nm (Fig. 4b).

To test the capability of the P1-2 Pdot for use in multi-excitation encoding applications, we allowed MCF-7 breast cancer cells to take up the P1-2 Pdot *via* endocytosis. Confocal fluorescence microscopy images of Pdot-labeled MCF-7 cells were acquired at different excitation wavelengths (Fig. 5). The cells were much brighter when excited with a 561 nm laser than with a 488 nm or 405 nm laser: the cell brightness ratio was 9.4 for $I_{561\ nm}/I_{488\ nm}$ and 12.5 for $I_{561\ nm}/I_{405\ nm}$ (Fig. S4†). These results are consistent with the single-particle flow results and indicate that the P1-2 Pdot possesses excitation selectivity and is suitable for use in multi-excitation-based fluorescence encoding.

3. Conclusions

Here we report an efficient 561 nm laser-excitable NIR Pdot, achieved *via* the novel use of a BODIPY unit as the primary absorber in a Pdot. This ternary D–ETU–A type Pdot exhibits simultaneously narrow absorption and emission bands, together with high single-particle brightness and a large Stokes shift. Due to the strong, narrow absorption around 551 nm, the Pdot is much brighter when excited by a 561 nm laser than when excited by a 488 nm or 405 nm laser. This property makes the Pdot can be utilized for selective yellow laser excited living cell imaging. Furthermore, we are trying to adopt this BODIPY-based D–ETU–A design strategy to develop 561 nm laser excited Pdot system with distinct emission spectra for multiplexed bioanalysis such as cell barcoding we previously reported[22] or mRNA-FISH application.

Conflicts of interest

The authors declare the following competing financial interests: D. T. Chiu and J. Yu have financial interest in Lamprogen Inc., which has licensed the technology from the University of Washington.

Acknowledgements

We gratefully acknowledge support of this work by the National Institutes of Health (R01MH115767) and the University of Washington.

References

1 C. Wu and D. T. Chiu, *Angew. Chem., Int. Ed.*, 2013, **52**, 3086.
2 J. Yu, Y. Rong, C.-T. Kuo, X.-H. Zhou and D. T. Chiu, *Anal. Chem.*, 2017, **89**, 42.
3 J. Li and K. Pu, *Chem. Soc. Rev.*, 2019, **48**, 38.
4 Q. Zhao, X. Zhou, T. Cao, K. Y. Zhang, L. Yang, S. Liu, H. Liang, H. Yang, F. Li and W. Huang, *Chem. Sci.*, 2015, **6**, 1825.
5 H.-S. Peng and D. T. Chiu, *Chem. Soc. Rev.*, 2015, **44**, 4699.
6 B. Bao, P. Su, Z. Yang, X. Zhai, J. Zhang, Y. Xu, Y. Liu, B. Gu and L. Wang, *Adv. Healthcare Mater.*, 2019, **8**, 1900255.
7 W. Tsai, C. Wang, C. Liao, a C. Yao, T. Kuo, M. Liu, C. Hsu, S. Lin, C. Wu, J. R. Pyle, J. Chen and Y. Chan, *Chem. Sci.*, 2019, **10**, 198.
8 T. Senthilkumar, L. Zhou, Q. Gu, L. Liu, F. Lv and S. Wang, *Angew. Chem., Int. Ed.*, 2018, **57**, 13114.
9 K. Zhang, Y. J. Gao, P. P. Yang, G. Bin Qi, J. P. Zhang, L. Wang and H. Wang, *Adv. Healthcare Mater.*, 2018, **7**, 1800344.
10 Z. Zhang, X. Fang, Z. Liu, H. Liu, D. Chen, S. He, J. Zheng, B. Yang, W. Qin, X. Zhang and C. Wu, *Angew. Chem., Int. Ed.*, 2020, **59**, 3691.
11 Y. Jiang and J. D. McNeill, *Nat. Commun.*, 2018, **9**, 4314.
12 Q. Zhang, Z. Zhang, X. Hu, J. Sun and F. Gao, *ACS Appl. Mater. Interfaces*, 2022, **14**, 179.
13 T. Li, M. Wu, Q. Wei, D. Xu, X. He, J. Wang, J. Wu and L. Chen, *Biomacromolecules*, 2023, **24**, 1943.
14 H. Gao, N. Zhang, J. Hu, J. Pan, Y. Cheng, H. Chen and J. Xu, *ACS Appl. Nano Mater.*, 2021, **4**, 7244.
15 X. Bai, K. Wang, L. Chen, J. Zhou and J. Wang, *J. Mater. Chem. B*, 2022, **10**, 6248.

16 M. Wu, Q. Wei, C. Xian, C. Dai, X. He, C. Wu, G. Sun and L. Chen, *Chin. Chem. Lett.*, 2023, **34**, 107867.
17 Q. Wei, D. Xu, T. Li, X. He, J. Wang, Y. Zhao and L. Chen, *Biosensors*, 2022, **12**, 1126.
18 L. Chen, D. Chen, Y. Jiang, J. Zhang, J. Yu, C. C. DuFort, S. R. Hingorani, X. Zhang, C. Wu and D. T. Chiu, *Angew. Chem., Int. Ed.*, 2019, **58**, 7008.
19 J. Zhang, J. Yu, Y. Jiang and D. T. Chiu, *ACS Appl. Mater. Interfaces*, 2022, **14**, 13631.
20 L. Chen, L. Wu, J. Yu, C. Kuo, T. Jian, I. Wu, Y. Rong and D. T. Chiu, *Chem. Sci.*, 2017, **8**, 7236.
21 L. Wu, I.-C. Wu, C. C. DuFort, M. A. Carlson, X. Wu, L. Chen, C.-T. Kuo, Y. Qin, J. Yu, S. R. Hingorani and D. T. Chiu, *J. Am. Chem. Soc.*, 2017, **139**, 6911.
22 F. Ye, C. C. White, Y. Jin, X. Hu, S. Hayden, X. Zhang, X. Gao, T. J. Kavanagh and D. T. Chiu, *Nanoscale*, 2015, **7**, 10085.
23 D. Wang, J. Liu, Z. Liu, Z. Zhang, Z. Sun, C. Wu and G. Wang, *ACS Appl. Nano Mater.*, 2020, **3**, 2214.
24 W. Xu, S. Lu, M. Xu, Y. Jiang, Y. Wang and X. Chen, *J. Mater. Chem. B*, 2016, **4**, 292.
25 Y. Rong, C. Wu, J. Yu, X. Zhang, F. Ye, M. Zeigler, M. E. Gallina, I. C. Wu, Y. Zhang, Y. H. Chan, W. Sun, K. Uvdal and D. T. Chiu, *ACS Nano*, 2013, **7**, 376.
26 C. T. Kuo, H. S. Peng, Y. Rong, J. Yu, W. Sun, B. Fujimoto and D. T. Chiu, *Anal. Chem.*, 2017, **89**, 6232.
27 C. S. Ke, C. C. Fang, J. Y. Yan, P. J. Tseng, J. R. Pyle, C. P. Chen, S. Y. Lin, J. Chen, X. Zhang and Y. H. Chan, *ACS Nano*, 2017, **11**, 3166.
28 S. Y. Liou, C. S. Ke, J. H. Chen, Y. W. Luo, S. Y. Kuo, Y. H. Chen, C. C. Fang, C. Y. Wu, C. M. Chiang and Y. H. Chan, *ACS Macro Lett.*, 2016, **5**, 154.
29 X. Zhang, J. Yu, Y. Rong, F. Ye, D. T. Chiu and K. Uvdal, *Chem. Sci.*, 2013, **4**, 2143.
30 R. Du, S. Cui, Z. Sun, M. Liu, Y. Zhang, Q. Wu, C. Wu, F. Guo and L. Zhao, *Chem. Commun.*, 2017, **53**, 8612.
31 I. C. Wu, J. Yu, F. Ye, Y. Rong, M. E. Gallina, B. S. Fujimoto, Y. Zhang, Y. H. Chan, W. Sun, X. H. Zhou, C. Wu and D. T. Chiu, *J. Am. Chem. Soc.*, 2015, **137**, 173.
32 C. P. Chen, Y. C. Huang, S. Y. Liou, P. J. Wu, S. Y. Kuo and Y. H. Chan, *ACS Appl. Mater. Interfaces*, 2014, **6**, 21585.
33 G. Hong, Y. Zou, A. L. Antaris, S. Diao, D. Wu, K. Cheng, X. Zhang, C. Chen, B. Liu, Y. He, J. Z. Wu, J. Yuan, B. Zhang, Z. Tao, C. Fukunaga and H. Dai, *Nat. Commun.*, 2014, **5**, 4206.
34 M. Liu, Z. Zhang, Y. C. Yang and Y. Chan, *Angew. Chem., Int. Ed.*, 2021, **60**, 983.
35 H. Pan, C. Wu, C. Lin, C. Hsu, Y. Tsai, P. Chowdhury, C. Wang, K. Chang, C. Yang, M. Liu, Y. Chen, S. Su, Y. Lee, H. K. Chiang, Y. Chan and P. Chou, *J. Am. Chem. Soc.*, 2023, **145**, 516.
36 M. Liu, T. Chen, J. R. Vicente, C. Yao, Y. Yang, C. Chen, P. Lin, Y. Ho, J. Chen, S. Lin and Y. Chan, *ACS Appl. Bio Mater.*, 2020, **3**, 3846.
37 H. Zhu, Y. Fang, X. Zhen, N. Wei, Y. Gao, K. Q. Luo, C. Xu, H. Duan, D. Ding, P. Chen and K. Pu, *Chem. Sci.*, 2016, **7**, 5118.
38 S. Wang, J. Liu, G. Feng, L. G. Ng and B. Liu, *Adv. Funct. Mater.*, 2019, **29**, 1808365.
39 H. Lu, J. Mack, Y. Yang and Z. Shen, *Chem. Soc. Rev.*, 2014, **43**, 4778.
40 C. Thivierge, A. Loudet and K. Burgess, *Macromolecules*, 2011, **44**, 4012.
41 A. Nagai and Y. Chujo, *Macromolecules*, 2010, **43**, 193.
42 G. Meng, S. Velayudham, A. Smith, R. Luck and H. Liu, *Macromolecules*, 2009, **42**, 1995.
43 V. R. Donuru, G. K. Vegesna, S. Velayudham, S. Green and H. Liu, *Chem. Mater.*, 2009, **21**, 2130.
44 S. R. Jung, R. Han, W. Sun, Y. Jiang, B. S. Fujimoto, J. Yu, C. T. Kuo, Y. Rong, X. H. Zhou and D. T. Chiu, *Anal. Chem.*, 2018, **90**, 6089.